Effect of Geothermal Brine Properties on Silica Scaling in Enhanced Geothermal Systems

Yung Ngothai[1,2], Daniel Lane[1], Gideon Kuncoro[1], Norio Yanagisawa[3], Peter Rose[4], and Allan Pring[2,5]

[1]School of Chemical Engineering, The University of Adelaide, SA
[2]South Australian Centre for Geothermal Energy Research, The University of Adelaide, SA
[3]Institute for Geo-Resources and Environment, Tsukuba, Ibaraki, Japan
[4]Energy and Geoscience Institute, The University of Utah, USA
[5]South Australian Museum, North Terrace, Adelaide, SA
yung.ngothai@adelaide.edu.au

Keywords

Amorphous silica, silica scaling, geothermal brine, pH, salinity, EGS

ABSTRACT

Silica scaling in Enhanced Geothermal Systems (EGS) is currently a concern affecting the economic viability of geothermal energy extraction. Knowledge of the effect of brine properties, such as pH and salinity, on silica scaling is essential for the effective design and operation of EGS reservoirs. This paper presents a laboratory study of silica scaling under variable environmental conditions.

A set of silica scaling experiments was conducted in Teflon-lined stainless steel autoclaves at 200ºC and saturated vapour pressure in order to simulate the conditions of a geothermal well in the Cooper Basin in South Australia. Tests were conducted in solutions supersaturated with respect to amorphous silica and in solutions supersaturated with respect to a granite sample extracted from the Habanero 3 well. Samples of stainless steel wire mesh were used as the platform for scale deposition. Colloidal silica concentrations of the reactant solutions were used to indicate the relative extent of silica scale deposition; these were calculated by the difference between the measured total dissolved and reactive silica concentrations. A scanning electron microscope was used. (i) to compare the relative surface coverage of the silica scale deposits and thus verify results from the reactant solution analysis; and (ii) to differentiate between different scale morphologies.

The rate of silica scale deposition was found to increase when Na ions were added to solution. Results from experiments used to determine the effect of Cl ions on the rate of silica scale deposition were inconclusive due to the dissolution of the wire mesh sheets. The extent of silica scaling was found to increase with increasing alkalinity. This trend contradicted the literature where a reduction in the extent of silica scaling at values of pH greater than 10 has been reported. This discrepancy could be due to a result of the high levels of silica supersaturation during autoclave quenching.

1. Introduction

A major concern affecting the economic viability of Enhanced Geothermal Systems (EGS) is the precipitation of amorphous silica in the circulated geothermal fluid (Gunnarsson & Arnorsson, 2005). Silica deposition severely limits the efficiency of power generation and the life of reinjection wells. It is responsible for several operational problems such as the tightening of reinjection wells and pipe blockages. The potential for silica deposition is dependent on the solubility of amorphous silica and factors that affect the solubility of amorphous silica in solution including temperature, pH, and ionic strength (Chan, 1989).

In many developed conventional geothermal fields, underground geothermal fluids are typically *undersaturated* with respect to amorphous silica. However, when geothermal fluids are extracted and cooled for electricity generation the solubility of amorphous silica is reduced such that the fluid becomes *supersaturated* and consequently capable of depositing silica as scale.

Gunnarsson and Arnórsson (2005) state that there are two processes involving aqueous silica that occur in amorphous silica supersaturated solution. The first process is the precipitation of monomeric silica directly onto surfaces. The second is the tendency for silica to polymerise and form colloids that remain in suspension for long periods of time. Polymeric silica is less likely to precipitate from solution than monomeric silica.

The dissolution of silica in water to form monosilicic acid (monomeric silica) occurs according to the following chemical reaction.

$$SiO_2(s) + 2H_2O \rightarrow H_4SiO_4(aq) \qquad [R1]$$

Reaction [1] occurs at the solid particle surface. The surface layer of silica containing hydrated *Si* atoms surrounded by *O* atoms are able to detach from the surface of the particle such that further formation of monosilicic acid can occur (Iler, 1955).

The silica saturation index (SSI) is often used to indicate the potential for silica scale deposition. It is defined as the ratio of silica concentration in the solution to the equilibrium solubility of amorphous silica. Silica scaling will only occur provided that SSI is greater than 1 and is generally not problematic for SSI

values <1.4, depending on temperature (Brown, 2011). Thus, to avoid amorphous silica scaling, it is common to inject geothermal water back into the well at a temperature above amorphous silica saturation. However, this method results in a relatively inefficient use of the heat energy brought to the surface.

Much work has been done to correlate the equilibrium solubilities of quartz and amorphous silica in water at different temperatures. There seems to be good agreement in the literature for temperatures below 300°C. Two correlations that agree well with the literature are provided as equations [1] and [2], respectively, where the solubility dependence of quartz and amorphous silica with temperature are described. Equation [1] was reported by Brown (2011) and equation [2] by Fournier & Rowe (1977).

$$\log C = -\frac{1309}{T} + 5.19 \qquad [E1]$$

$$\log C = -\frac{731}{T} + 4.52 \qquad [E2]$$

where C is the concentration of silicic acid (mg/kg) and T is the absolute temperature in Kelvin. Both equations are valid for systems at a temperature of 0-250°C.

The equilibrium solubilities of quartz and amorphous silica are both dependent on particle size. Equations (1) and (2) are both limited in that they do not account for differences in particle size. Iler (1955) reported a 300% decrease in the solubility of amorphous silica for a decrease in particle diameter from 100µm to 10µm at 25°C. However, the dependence of solubility on particle size is only significant for small particles. For particle diameters greater than 100µm, large differences in particle size results in only marginal changes in solubility.

Previous work done in the field of silica scaling in EGS does not adequately account for differences in brine properties at elevated temperature (i.e., T>150°C). To do this, experiments were conducted using granite samples from the Habanero 3 (HAB 3) well, a site in the Cooper Basin of Australia, as well as using gelatinous (amorphous) silica. The granite samples are from drill cuttings from the bottom of a 5km deep borehole.

The aim of the experiments was to investigate the effect of various brine properties on silica deposition at a high degree of supersaturation (37 times SSI) with respect to amorphous silica at 200°C. The experiments were undertaken to determine the following aspects.

- The effect of Na and Cl ions on the rate of silica scale deposition in solutions containing gelatinous silica supersaturation;
- The effect of pH on the extent of silica scale deposition in solutions containing gelatinous silica; and
- The rate of silica scale deposition in solutions containing rock sampled from the HAB 3 well in the Cooper Basin.

2. Experimental

2.1 Description of Experiments

Five sets of experiments were conducted. They are summarised in Table 1.

Solute(s) were mixed with 14ml of the solvent inside Teflon tubes with internal capacities of 18ml. All experiments were conducted at 200°C and saturated vapour pressure (16 bar) inside an insulated oven. Headroom of 4ml was allowed in the Teflon tubes for thermal expansion. A square piece of 316-stainless steel wire mesh was inserted in each Teflon tube to act as the platform for scale deposition. The Teflon tubes were then fitted inside the stainless steel autoclaves to be tested at the elevated temperature and pressure. Experiments A to D each consisted of six tests corresponding to reaction times of 1, 7, 14, 21, 28 and 56 days, plus a control test with a 56 day reaction period. The control test (filled with only Milliq water) was used to check for any dissolution and contamination of the wire mesh. Experiment E consisted of four tests which all had reaction times of 28 days. Four readily available buffer solutions were used to adjust the pH in experiment E. The pH of each buffer solution was measured before use. The buffer solutions used and their measured pH values are provided in Table 2.

Table 2. Buffer solutions used in experiment E.

Test	Buffer Solution	Measured pH
E1	Acetate buffer	3.94
E2	Phosphate buffer	6.92
E3	NaH_2PO_4 buffer	10.70
E4	KCl and NaOH buffer	12.52

Table 1. Summary of Experiments.

Exp.	Tests	Purpose	Solvent	Solute(s)
A	A1, A2, A3, A4, A5, A6, AC	To determine the rate of silica scale deposition in solutions supersaturated with respect to amorphous silica	Milliq water	Silica gel (35.7g/L)
B	B1, B2, B3, B4, B5, B6, BC	To determine the effect of Na ions on the rate of silica scale deposition	Milliq water	$NaHCO_3$ (357 ppm) and silica gel (35.7g/L)
C	C1, C2, C3, C4, C5, C6, CC	To determine the effect of Cl ions on the rate of silica scale deposition	Milliq water	$CaCl_2 \cdot 2H_2O$ (376 ppm) and silica gel (35.7g/L)
D	D1, D2, D3, D4, D5, D6, DC	To determine the rate of silica scale deposition in solutions with HAB 3 rock	Milliq water	HAB 3 rock sample (35.7g/L)
E	E1, E2, E3, E4,	To determine the effect of solution pH on the extent of silica scale deposition	Buffer solutions	Silica gel (35.7g/L)

At the end of each test, the autoclaves were quenched in cold water for 15 minutes prior to aqueous sampling. All aqueous samples were subjected to pH measurement and then preserved in 4% nitric acid to prevent further silica precipitation. All aqueous samples were later analysed for reactive and total dissolved silica. The HACH silicomolybdate method was used to measure the reactive silica (H_4SiO_4) for all experiments, while Inductively Coupled Plasma Optical Emission Spectroscopy (ICPOES) was used to measure the total dissolved silica for experiments B, C and E. Total dissolved silica for experiments A and D was calculated using the empirical dissolution rate correlations developed by Rimstidt and Barnes (1980) and by Robinson (1982).

After aqueous sampling, the wire mesh sheets were removed from the Teflon tubes and dried in an oven at 80°C. The wire mesh sheets were later used for morphological studies of silica deposition by scanning electron microscopy (SEM).

2.2 Sample Preparation

2.2.1 Preparation of Amorphous Silica Particles

80g of coarse silica beads were crushed to 100µm – 200µm. The crushed sample was then subject to size classification using a cylindrical sieve. Particles collected between sieve trays with aperture sizes 100µm and 200µm were then removed for washing to remove any fines that adhered to the particles. Fines have a significant effect on both the rate and on the extent of silica dissolution (Robinson 1982). Their removal is essential in order to obtain reliable results. To remove the fines, silica particles were washed in batches of 5g at a time in an ultrasonic bath. The 5g portions were added to 200ml of Milliq water and washed for 15 minutes. Each portion was washed three times with fresh Milliq water. Washed silica particles were dried in an oven for 24 hours at 120°C and then stored in a desiccant bed as stock, until needed, to prevent hydration of the particles. The surface areas of the ultrasonically cleaned silica particles were measured using N_2-BET.

Silica particles used in this study were greater than 100µm. It was therefore expected that particle size would not have had a significant influence on the equilibrium solubility.

2.2.2 Preparation of Habanero 3 Rock Sample

The Habanero 3 rock sample taken from drill cuttings was prepared using the same process as was used to prepare the amorphous silica particles.

2.2.3 Preparation of the Stainless Steel Mesh

A square piece of stainless steel mesh (10mm x 10mm) was required as the platform for scale deposition for each experiment. A 300mm x 200mm length of the mesh was wet sanded to remove impurities. A steady flow of water was applied during sanding to ensure that detached pieces of the mesh were washed away so that they did not remain attached to the mesh. The mesh was then dried at 80°C for 24 hours before being cut into square pieces. Each mesh was pre-weighed before being used in the precipitation reaction.

2.2.4 Preparation of the $NaHCO_3$ Solution and the $CaCl_2.2H_2O$ Solution

Aqueous solutions containing $NaHCO_3$ and $CaCl_2.2H_2O$ were prepared for experiments B and C, respectively. The two salt solutions were prepared before adding the silica particles. 5mg of $NaHCO_3$ powder was dissolved in 14ml of Milliq water to prepare a $NaHCO_3$ solution of concentration 357ppm. This solution contained the same concentration of Na ions as a 250ppm NaCl solution. Similarly, 5.3 mg of $CaCl_2.2H_2O$ was dissolved in 14ml of Milliq water to prepare a $CaCl_2.2H_2O$ solution of concentration 376ppm. The concentration of this solution contained the same number of Cl ions as a 250ppm NaCl solution.

3. Results and Discussion

Silica deposition was found to occur on most of the wire mesh plates. However, dissolution of the wire mesh itself meant that the mass of silica scale deposited could not be calculated directly. There was clear evidence that the wire mesh plates had corroded in all experiments, even in the control test experiments. This could be due to deionised water is corrosive at high temperature. A reduction in the mass of the wire mesh plates used in control tests was measured for all experiments. SEM images of the wire mesh samples confirmed iron oxide scale particles; iron oxide scale has a different morphology than silica scale. Usually the deposited silica colloids were globular in shape and the iron oxide particles tabular. Corrosion of the wire mesh was not expected, especially in experiments A and D where deionised water was used as the solvent, given that the mesh was made of 316-stainless steel. An X-ray spectrum of the wire mesh indicated a high proportion of nickel in the alloy which may have caused the rapid rate of corrosion. Corrosion was most severe in experiment C, presumably due to the activity of Cl ions in the solution. Over the duration of experiment C (56 days) the wire mesh as shown in Figure 1 had decayed to 14.2% of its original mass. The result of the stainless steel corroding is important in itself, and shows that material selection is a very important design process, as it is necessary to choose appropriate high quality stainless steels for pumps and equipment when the project gets underway.

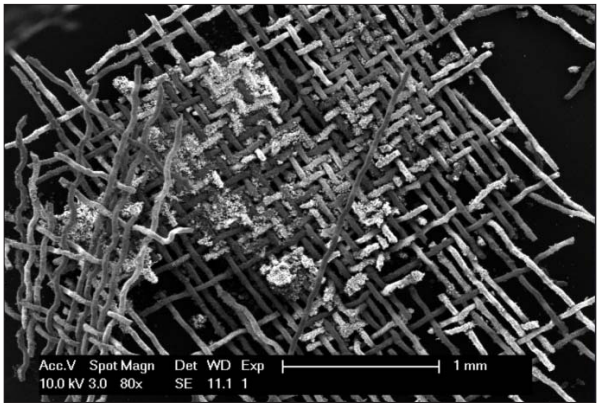

Figure 1. Wire mesh from experiment C after 56 days.

As a consequence of corrosion, quantitative analysis was limited to that of the aqueous samples. The wire mesh samples were used only to verify the results obtained from analysis of the solution samples. Despite the presence of corrosion products, it was generally obvious where silica deposition was more prevalent when observing the wire mesh samples from the SEM images.

3.1 Effect of Na Ions and Cl Ions on the Solubility of Silica

It was found that the presence of both Na ions and Cl ions caused a decrease in total dissolved silica (Figure 2). Total dissolved silica in deionised water (experiment A) was calculated using the Rimstidt and Barnes (1980) rate model. The reduced solubility of total dissolved silica when Cl or Na ions were

added to the silica solution is consistent with work by Makrides et al., (1979) who explained due to increase in ionic strength or electrostatic interaction and consequently cause a decrease in the solubility of silica.

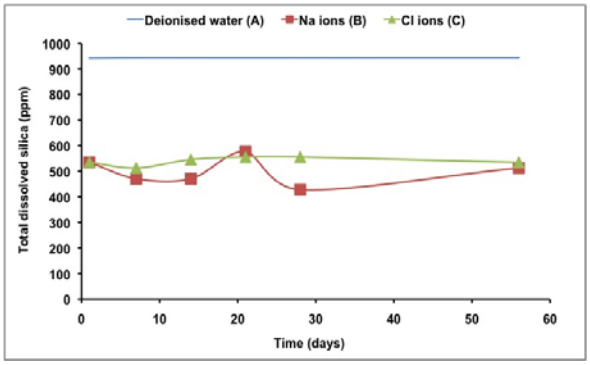

Figure 2. Effect of Na and Cl ions on the solubility of total dissolved silica.

Figure 3 shows the rate of disappearance of reactive silica while Figure 4 shows the rate of colloidal silica in the solutions for three different solvents. The reduction rates (Figure 3) can be explained due to silica polymerisation that leads to the formation of the colloidal particles (Figure 4). The concentration of colloidal silica was calculated by assuming it to be equal to the difference between the total dissolved and reactive silica.

By comparison of the slope of the red curve (Na ions) and the slope of the blue curve (deionised water) in Figure 4, it can be seen that the rate of change in colloidal silica concentration and consequently the rate of colloid formation was made greater by

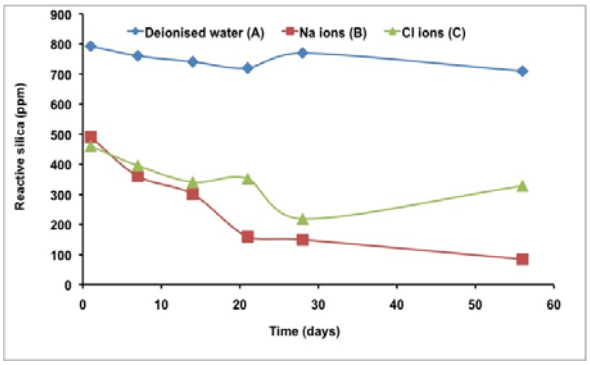

Figure 3. Effect of Na and Cl ions on the rate reactive silica.

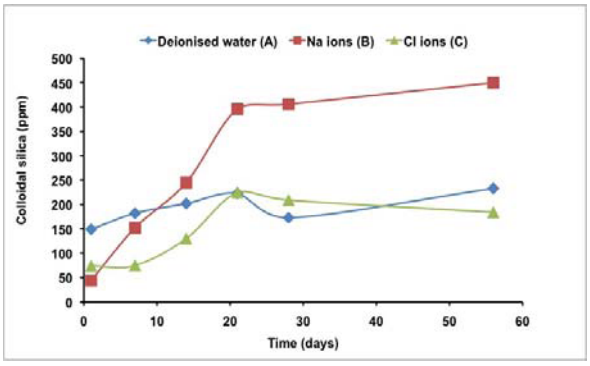

Figure 4. Effect of Na and Cl ions on the rate of the colloidal silica.

adding Na ions to the reactant solution. This trend only indicates a potential increase in the rate of silica scaling since the rate of change of colloidal silica is not proportional to the precipitation rate of silica colloids. The formation of silica colloids occurs via the following three stages. *nucleation*, *ripening* and *growth* (Brown, 2011). During *nucleation,* silicilic acid molecules react to form monomers and polymers. The polymerisation reaction continues to occur until the number of monomeric silica particles is reduced to a level whereby further nucleation is prevented. At this stage *ripening* occurs. During ripening smaller particles dissolve in solution to reform monomeric silica particles such that the larger particles can continue to grow in size. During the *growth,* phase available monomeric particles latch on to larger particles. Typical silica colloids are between 0.003µm and 3µm in diameter and can take the form of sols, aggregates or gels. Therefore, if silica colloids are sufficiently small a high proportion of the colloids can exist in suspension with few colloids depositing as scale (Makrides et al., 1979).

SEM analysis showed that silica colloids were of the order of 1µm when Na ions were added to solution (Figure 5) and of the order of 0.2µm (Figure 6) when deionised water was used as the solvent. Given that the size of the silica colloids was greater in the solutions containing Na ions, it is unlikely that the colloids in the deionised water would have had a greater tendency to settle than the colloids in the solution containing the Na ions.

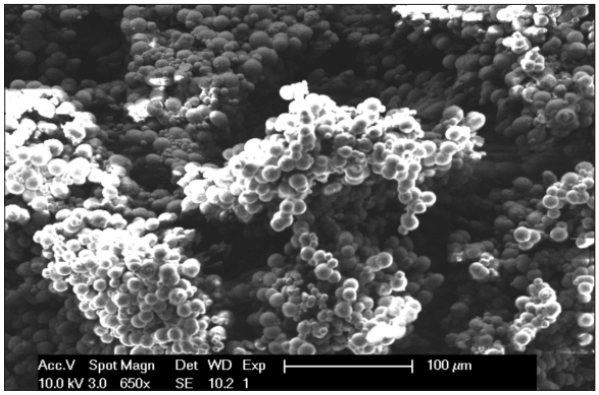

Figure 5. SEM image of wire mesh from experiment B6 (Na ions – 56 days).

The increased rate of scale deposition when Na ions were added to the reactant solution was verified by the SEM analysis and is consistent with the literature (Brown, 2011 and Makrides et al., 1979). Wire mesh samples from solutions containing Na ions showed significantly more silica scaling at any given time than the wire mesh samples from deionised water. From SEM images as shown in Appendix B, it appears the nucleation phase occured around day 1, ripening between day 1 to 7, and growth after 14 days.

According to Brown (2011), the increased rate of silica scale deposition when Na ions are in solution is a result of electrostatic interactions between the negatively charged silica colloids and the positively charged Na ions, which interact to reduce the repulsive barrier that resists colloid agglomeration. The reduced silica solubility in the solution containing Na ions would have also contributed to the increased rate in silica scaling by increasing the extent of supersaturation. The extent of supersaturation of

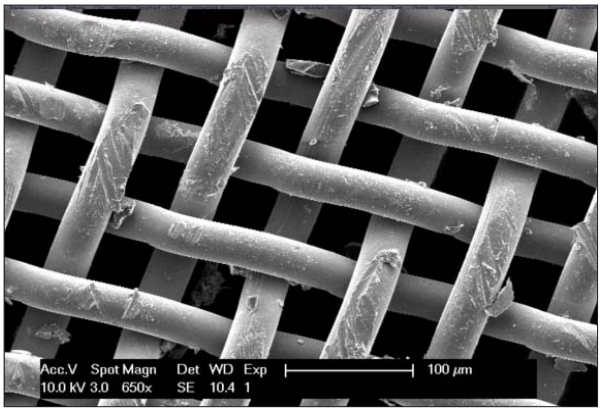

Figure 6. SEM image of wire mesh from experiment A6 (deionised water - 56 days).

amorphous silica has been found to significantly affect the rate of silica scaling (Makrides et al., 1979).

The presence of Cl ions in solution caused a small increase on polymerisation rates of silica, as can be seen by comparison of the slope of the green curve (Cl ions) and the slope of the blue curve (deionised water) in Figure 4. According to Makrides et al., (1979), the addition of a small amount of chloride in the solution has comparatively little effect on polymerisation rate; however, a large amount of chloride increases the supersaturation of silica and therefore leads to a higher polymerisation rate. It is noted that the polymerisation rate appears to remain constant after 21 days. However, the results from the reactant solution analysis are inconclusive without knowledge of the relative colloid settling tendencies in solutions containing Cl ions and in deionised water. Reliable comparison of silica scale coverage from solutions containing Cl ions with mesh samples from deionised water was not feasible due to the large coverage of rust scale on the mesh samples from solutions containing Cl ions (Figure 7). As mentioned earlier, corrosion of the stainless steel wire mesh was not expected, however it occurred for all cases and was most severe in experiment C. This corrosion led to the generation of cations such as Fe ions in solution, and these then can act as a bridge between neighbouring colloid particles, essentially bonding them together to form a scale or a larger agglomerate that is gravitationally deposited.

Figure 8 shows variation of pH with time for experiments A to C. The constant rise in pH for experiment B (Na ions) is consistent with the result in Figure 4 where the rate of polymerisation increase would lead to an increase in pH. Similar results have been observed by Rothbaum and Rohde (1979), where the rise of pH during the polymerisation of silica can be explained due to hydrolysis of polymers (i.e., monosilicic acid is a stronger acid than polysilcic acid). The rise and fall in pH for experiments A (deionised water) and C (Cl ions) could be attributed to polymerisation and depolymerisation.

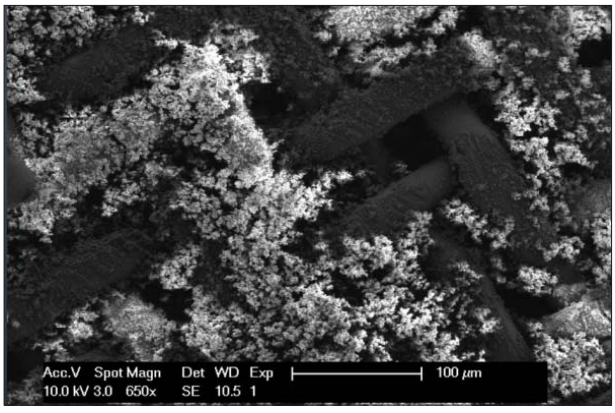

Figure 7. SEM image of wire mesh from experiment C6 (Cl ions – 56 days).

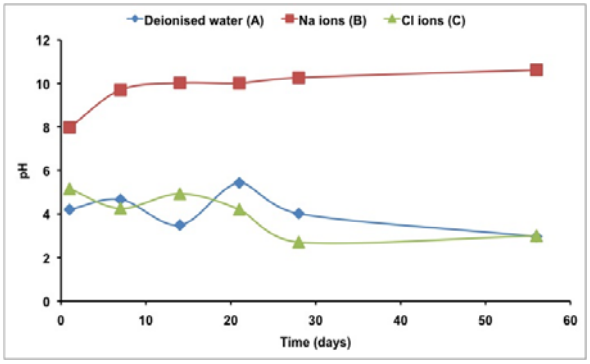

Figure 8. Variation of pH during polymerisation of silica solutions.

3.2 Effect of pH

On increasing alkalinity above pH 7 the concentration of total dissolved silica increased at an increasing rate as can be seen by inspection of Figure 9. This finding is consistent with work by Iller (1955), Henley (1983) and Brown (2011). They reported an increase in silica solubility with increasing pH. According to Brown (2011) the increasing trend above pH 7 is a result of the dissociation of silicic acid to form the silicate ion ($H_3SiO_4^-$) which is significantly more soluble than silicic acid, as described by reaction 2.

$$H_4SiO_4 \longleftrightarrow H^+ + H_3SiO_4^- \qquad [R2]$$

It was found that the total dissolved silica concentration at pH 12.5 was 590% higher than at pH 10.7. It is expected that this finding was a result of the dissociation of $H_3SiO_4^-$ to form $H_2SiO_4^{2-}$ which is significantly more soluble again, as described by reaction 3. According to Henley (1983) this second dissociation reaction is only significant above pH 11.

$$H_3SiO_4^- \longleftrightarrow H^+ + H_2SiO_4^{2-} \qquad [R3]$$

Total dissolved silica concentrations below pH 7 were lower than expected. Henley (1983) found that below pH 7 the solubility of amorphous silica is virtually independent of pH. It was therefore expected that total silica concentrations below pH 7 would be the same as the solubility of amorphous silica in deionised water. The concentration of amorphous silica in pure water was calculated to be 942ppm using the rate model developed by Rimstidt and Barnes (1980). The expected values are 293% and 96% higher than the experimental total silica concentration values at pH 3.9 and pH 6.9 respectively. It is suspected that an error in total dissolved silica concentration measurements was responsible for this discrepancy. Had the test tubes containing the solution samples for total dissolved silica analysis not been sufficiently shaken to transfer the settled silica colloids back into suspension the settled colloids would not have been detected in the ICP-OES measure-

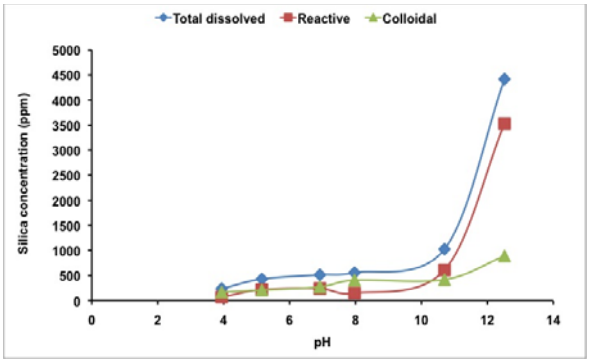

Figure 9. Effect of pH on total, reactive and colloidal silica concentration (experiment E - 28 days).

ments. Consequently, the total silica measurements would have been lower than their true values.

It was found that the concentration of colloidal silica in suspension increased slightly with rising pH which indicates an increase in silica scale deposition. Again it is emphasised that this trend only indicates higher levels of scale deposition as the silica colloids may have had different settling tendencies at the different pH values. However, SEM analysis showed the deposited silica colloids to be of similar size over the range of pH values tested and, therefore, it is likely that they had similar settling tendencies.

Figures 10 to 13 illustrate the relative differences in morphology of silica scale surface coverage at different values of pH from SEM analysis. SEM images verified the increase in silica scale deposition with increasing pH. Silica scale coverage was more dense at pH 12.52. Scale coverage was so dense that only small sections of the wire mesh could be seen beneath the deposited layer. Scale coverage was less dense but still significant at pH 10.7 and at pH 6.9. At pH 3.9, virtually no scale was deposited on the wire mesh sheet. This could be due to retardation of polymerisation at low pH.

An X-ray spectrum of the plate-like scale structures depicted on the mesh sample corresponding to pH 10.7 in Figure 12 gave *P* and *O* as major peaks and *Si* as a minor peak indicating that the phosphate ions in the buffer solution reacted with silica to form a scale complex consisting of both phosphorus and silica.

The trend of increasing scale deposition with increasing pH was not expected. The trend did not agree with experiments conducted by Henley (1983) which showed relatively less silica scale deposition at pH 11 than at pH 7 and virtually no deposition at pH 13. It is suspected that differences between experiments resulted in this discrepancy. All of the reactant solutions appeared to be supersaturated with respect to amorphous silica after quenching even for the test at pH 12.5. This was most likely a result of adding excessively high amounts of amorphous silica gel to reactant solutions at the start of each reaction. Henley (1983), on the other hand, reported that above approximately pH 11, solutions became undersaturated with respect to amorphous silica after flashing and therefore not able to deposit silica as scale. The low level of scale deposition at pH 3.9 was most likely due to the slow kinetics of precipitation at that pH. It is expected that the reaction was far from equilibrium.

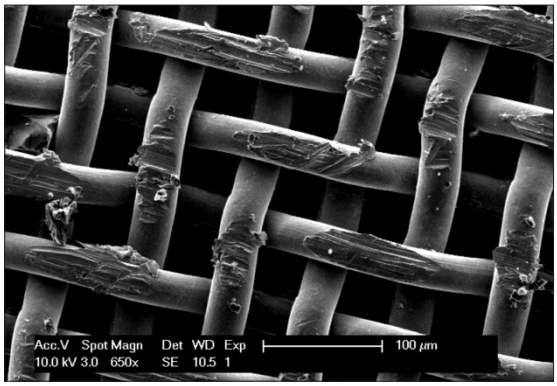

Figure 10. SEM image of wire mesh at pH 3.94 (Experiment E1 - 28 days).

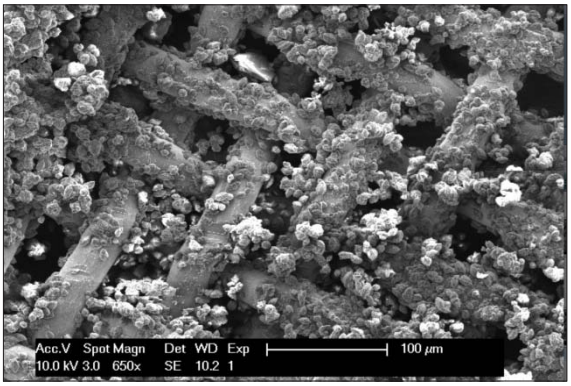

Figure 11. SEM image of wire mesh at pH 6.92 (Experiment E2 - 28 days).

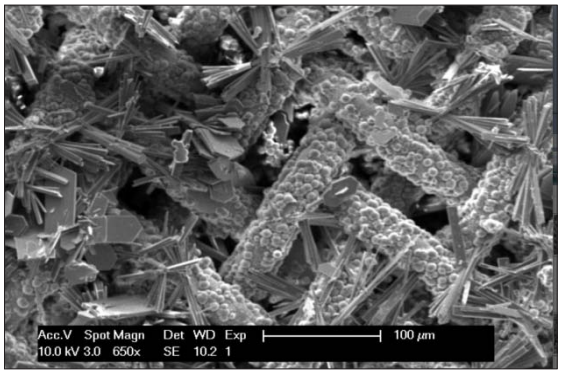

Figure 12. SEM image of wire mesh at pH 10.7 (Experiment E3 - 28 days).

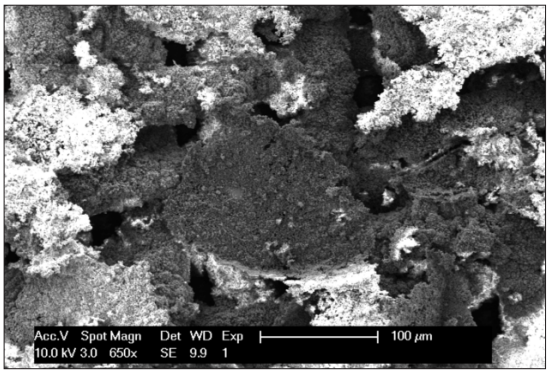

Figure 13. SEM image of wire mesh at pH 12.52 (Experiment E4 - 28 days).

3.3 Dissolution of Granite Sample From Habanero 3 Well

Figure 14 shows the dissolution rate of silica for the granite sample from HAB 3 well. The solid line represents the total dissolved silica which was calculated using correlations developed by Rimstidt and Barnes (1980) and by Robinson (1982). The rate model predicts that the concentration of dissolved silica from the HAB 3 granite sample has reached 14.5% of the equilibrium solubility after 1 day and just over 95% after 3 weeks. This indicates the kinetics of quartz dissolution in water is significantly lower than the kinetics of amorphous silica dissolution in water (experiment A). As noted earlier, the Robinson (1982) rate model used to predict the dissolution of the HAB 3 granite sample was limited by the assumption that the sample followed the same dissolution behaviour as pure quartz. However, the HAB 3 granite sample primarily consisted of quartz (approximately 70%) with the remainder consisted of albite and K-feldspar. The latter minerals not only have faster kinetics than quartz but also have greater solubilities at 200ºC. Therefore it is expected that both the rate of dissolution and the equilibrium solubility predicted for this HAB 3 granite sample were underestimated.

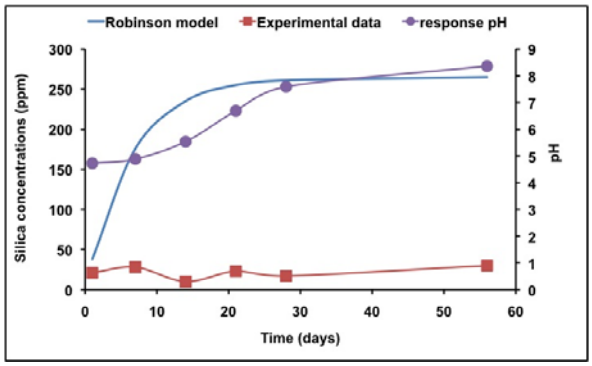

Figure 14. Silica concentration versus time response of granite sample from the HAB 3 well.

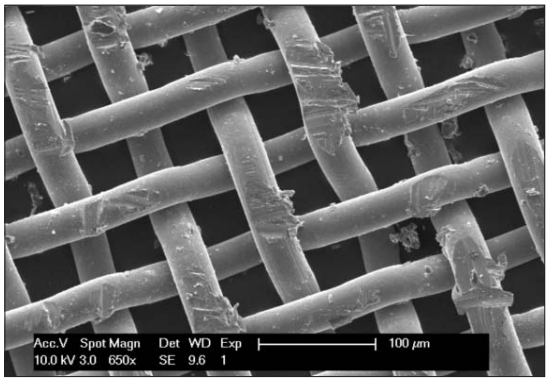

Figure 15. SEM image of wire mesh from experiment D (HAB 3 sample - 1 day).

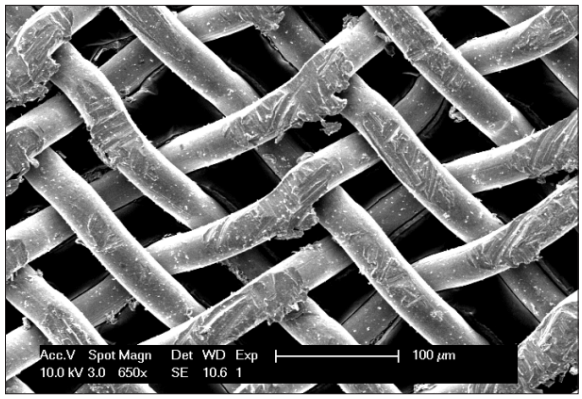

Figure 16. SEM image of wire mesh from experiment D (HAB 3 sample - 56 days).

Figure 14 also shows the experimental data which represents the reactive silica in the solution. There is insignificant change in terms of the rate of reactive silica. The measured reactive silica concentrations were much lower as compared to the predicted model. This could be due to polymerisation over the reaction period and can be confirmed by examining the change in pH as well as SEM analysis. The measured pH was found to rise from 4.73 for day 1 to 8.36 after 56 days. SEM images for day 1 and day 56 are shown in Figures 15 and 16 to demonstrate slight polymerisation.

4. Conclusion

The aim of this study was to determine the effect of brine properties on silica scaling. However, dissolution of the stainless steel wire mesh sheets prevented the direct measurement of the mass of the silica scale deposits. The concentration of colloidal silica was used to indicate the relative severity of silica scaling and SEM analysis was used to verify the analysis of the reactant solutions. Reactant solution analysis indicated that the presence of Na ions increased the rate of silica scale deposition; SEM analysis verified this. The results used to determine the effect of Cl ions in solution on the rate of silica scaling were inconclusive. Rust particles covered much of the silica scale deposits, preventing the comparison of samples from the wire mesh. The extent of silica scale deposition was found to increase with rising pH. This trend did not agree with experiments conducted by Henley (1983) who found silica scaling to be negligible above pH 11. It is expected that this discrepancy was due to a high level of amorphous silica supersaturation during quenching. No significant change in the rate of silica scaling was observed when the HAB 3 rock sample was used as the solute. It is expected that this was due to the HAB 3 rock sample having a lower solubility than the amorphous silica.

5. References

Brown K., 2011. "Thermodynamics and Kinetics of Silica Scaling", Proceedings from the International Workshop on Mineral Scaling, 25-27 May 2011, Manila, p. 1-7.

Chan S.H., 1989. "A review on solubility and polymerisation of silica", Geothermics, v. 18, p. 49-56.

Fournier R.O. and J.J. Rowe, 1977. "The solubility of amorphous silica in water at high temperatures and pressures", American Mineralogist, v. 62, p. 1052-1056.

Gunnarsson I. and S. Arnorsson, 2005. "Impact of silica scaling efficiency of heat extraction from high temperature geothermal fluids", Geothermics, v. 34, p. 320 – 329.

Henley R., 1983. "pH and Silica Scaling Control in Geothermal Field Development", Geothermics, v. 12, n. 4, p. 307–321.

Iler R., 1955. "The Colloid Chemistry of Silica and Silicates", Cornell University press, New York.

Makrides A., M. Turner, and J. Slaughter, 1979. "Condensation of Silica from Supersaturated Silicic Acid Solutions", Journal of Colloid and Interface Science, v. 73, n. 2, p. 379–402.

Marshall W. and J. Warakomski, 1980. "Amorphous Silica Solubilities – II. Effect of Aqueous Salt Solutions at 25ºC", Geochemica et Cosmochimica Acta, v. 44, p. 915–924.

Marshall W., 1980. 'Amorphous Silica Solubilities – III. Activity Coefficient Relations and Predictions of Solubility Behaviour in Salt Solutions, 0-350ºC', Geochemica et Cosmochimica Acta, v. 44, p. 925–931.

Rimstidt J. and H. Barnes, 1980. "The Kinetics of Silica-Water Reactions", Geochemica et Cosmochimica Acta", v. 44, p. 1683–1699.

Robinson B., 1982. "Quartz Dissolution and Silica Deposition in Hot Dry Rock Geothermal Systems", Thesis, Massachusetts Institute of Technology, Cambridge.

Rothbaum H.P. and A.G. Rhode, 1979. "Kinetics of silica polymerization and deposition from dilute solutions between 5 and 180°C", Journal of Colloid & Interface Science, v. 71, p. 533–559.

APPENDIX

Experiment A

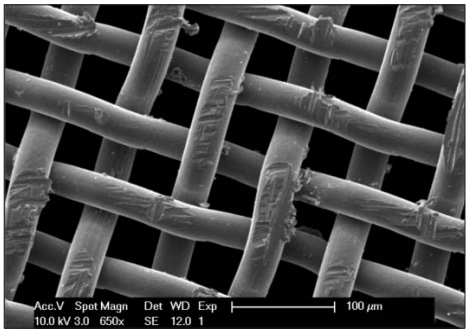

Figure A1. SEM image of wire mesh from Test A1.

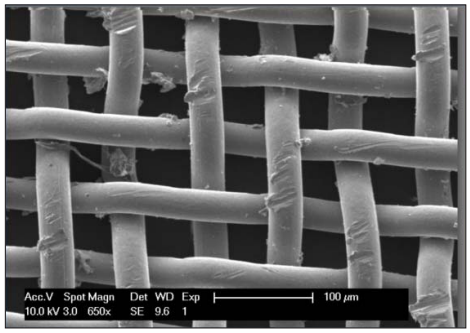

Figure A2. SEM image of wire mesh from Test A2.

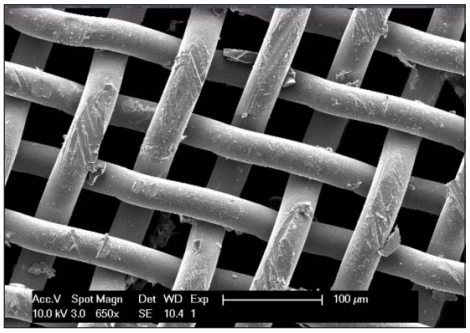

Figure A3. SEM image of wire mesh from Test A3.

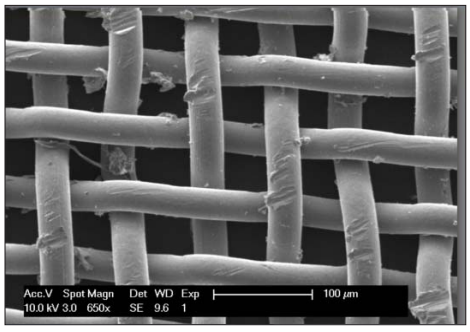

Figure A4. SEM image of wire mesh from Test A4.

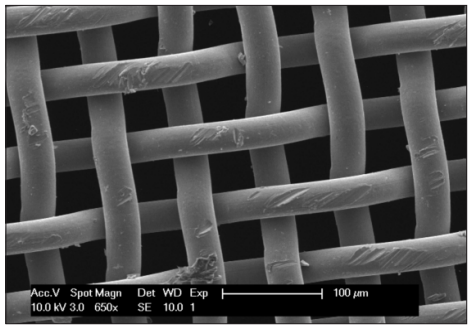

Figure A5. SEM image of wire mesh from Test A5.

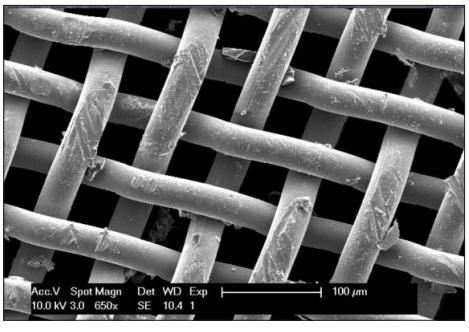

Figure A6. SEM image of wire mesh from Test A6.

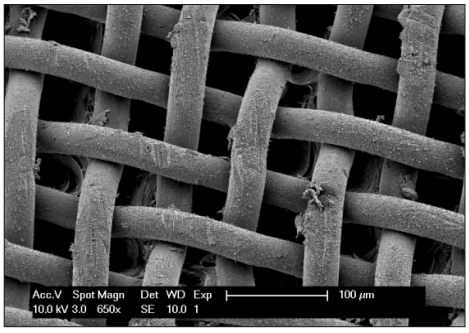

Figure A7. SEM image of wire mesh from Test AC.

Experiment B

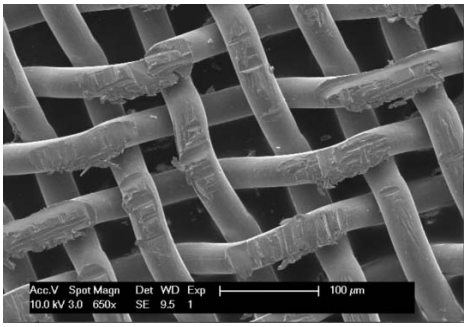

Figure B1. SEM image of wire mesh from Test B1.

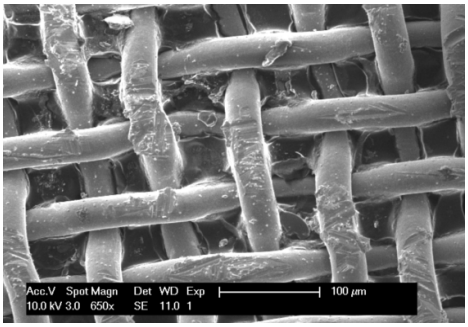

Figure B2. SEM image of wire mesh from Test B2.

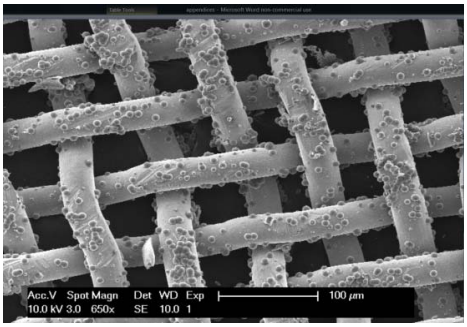

Figure B3. SEM image of wire mesh from Test B3.

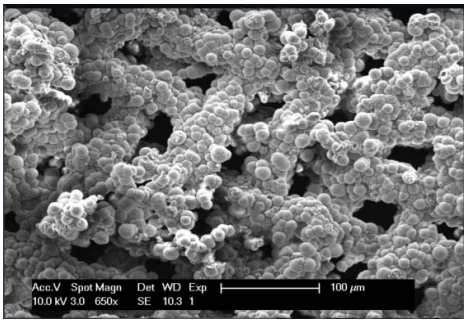

Figure B4. SEM image of wire mesh from Test B4.

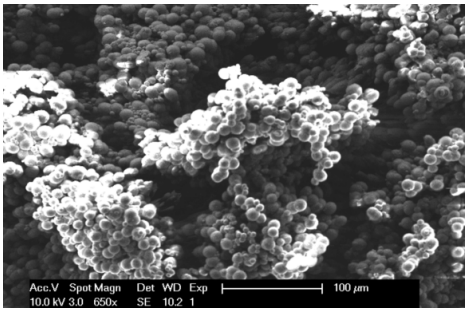

Figure B5. SEM image of wire mesh from Test B5.

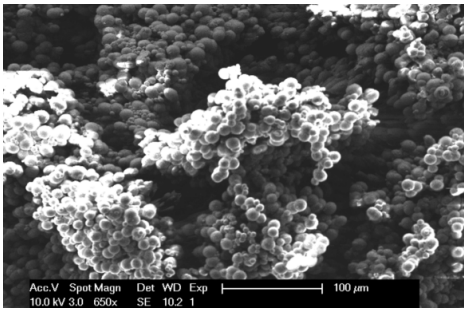

Figure B6. SEM image of wire mesh from Test B6.

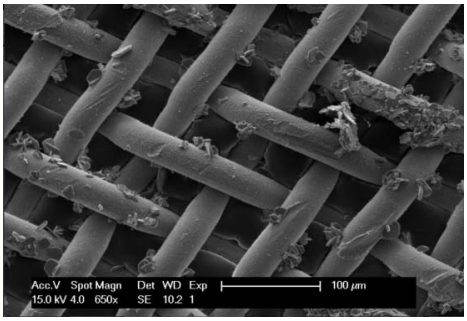

Figure B7. SEM image of wire mesh from Test BC.

Experiment C

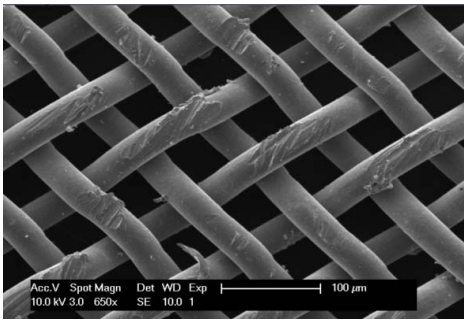

Figure C1. SEM image of wire mesh from Test C1.

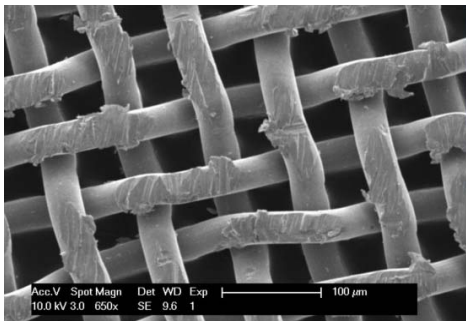

Figure C2. SEM image of wire mesh from Test C2.

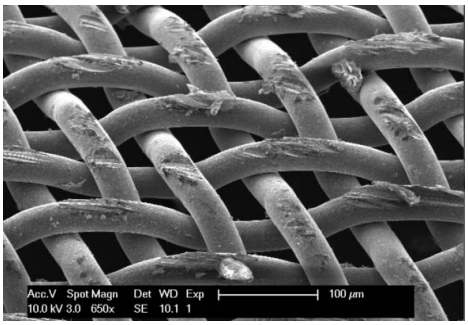

Figure C3. SEM image of wire mesh from Test C3.

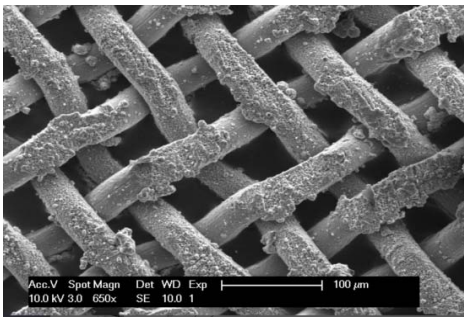

Figure C4. SEM image of wire mesh from Test C4.

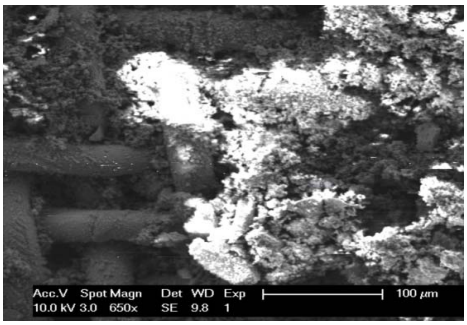

Figure C5. SEM image of wire mesh from Test C5.

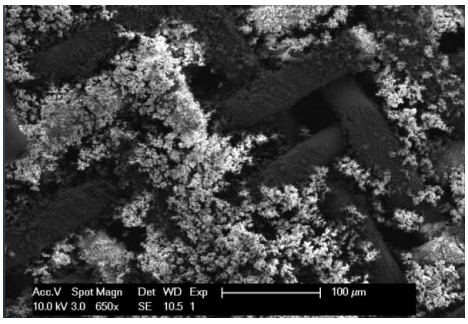

Figure C6. SEM image of wire mesh from Test C6.

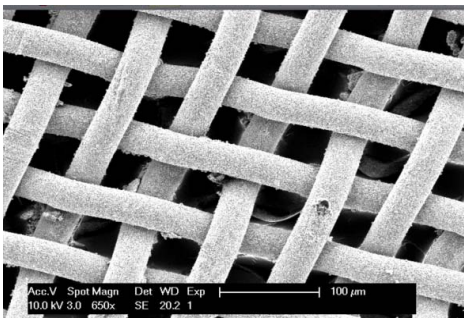

Figure C7. SEM image of wire mesh from Test CC.

Experiment D

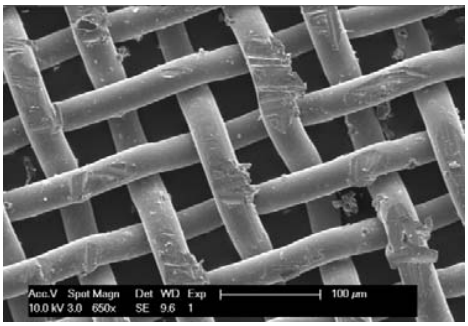

Figure D1. SEM image of wire mesh from Test D1.

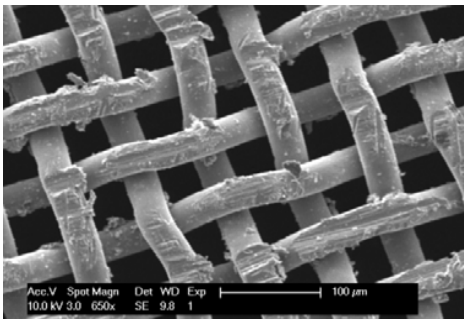

Figure D2. SEM image of wire mesh from Test D2.

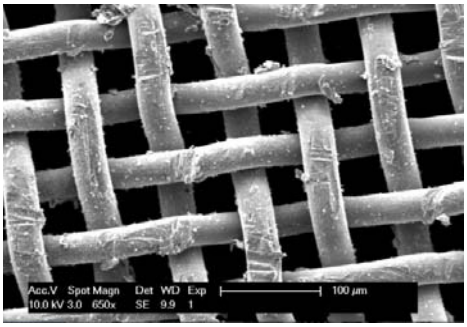

Figure D3. SEM image of wire mesh from Test D3.

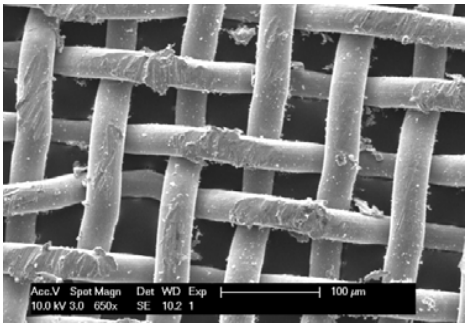

Figure D4. SEM image of wire mesh from Test D4.

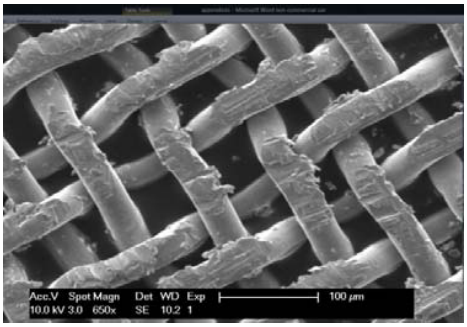

Figure D5. SEM image of wire mesh from Test D5.

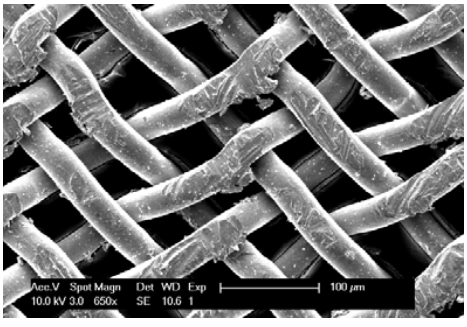

Figure D6. SEM image of wire mesh from Test D6.

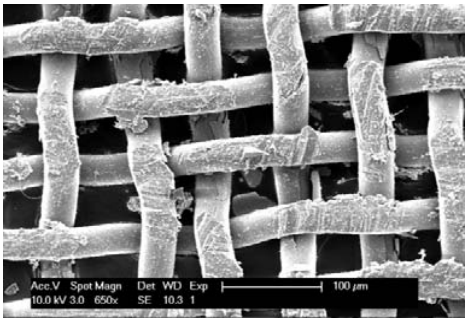

Figure D7. SEM image of wire mesh from Test DC.